HHS Public Access

Author manuscript

Neuron. Author manuscript; available in PMC 2020 December 04.

Published in final edited form as:

Neuron. 2019 December 04; 104(5): 931–946.e5. doi:10.1016/j.neuron.2019.08.035.

Pum2 shapes the transcriptome in developing axons through retention of target mRNAs in the cell body

José C. Martínez[1,2], **Lisa K. Randolph**[2,3], **Daniel Maxim Iascone**[3,4], **Helena F. Pernice**[2,5], **Franck Polleux**[4,6,7], **Ulrich Hengst**[2,8,9,*]

[1]Medical Scientist Training Program, Columbia University Irving Medical Center, New York, NY 10032, USA

[2]The Taub Institute for Research on Alzheimer's Disease and the Aging Brain, Vagelos College of Physicians and Surgeons, Columbia University, New York, NY 10032, USA

[3]Doctoral Program in Neurobiology and Behavior, Columbia University, New York, NY 10027, USA

[4]Mortimer B. Zuckerman Mind Brain Behavior Institute, Columbia University, New York, NY 10027, USA

[5]Department of Anatomy and Cell Biology, Biomedical Center, Medical Faculty, Ludwig-Maximilians-University, 82152 Planegg-Martinsried, Germany

[6]Department of Neuroscience, Vagelos College of Physicians and Surgeons, Columbia University, New York, NY 10027, USA

[7]Kavli Institute for Brain Science, Columbia University, New York, NY 10027, USA

[8]Department of Pathology and Cell Biology, Vagelos College of Physicians and Surgeons, Columbia University, New York, NY 10032, USA

[9]Lead Contact

SUMMARY

Localized protein synthesis is fundamental for neuronal development, maintenance, and function. Transcriptomes in axons and soma are distinct but the mechanisms governing the composition of axonal transcriptomes and their developmental regulation are only partially understood. We found that the binding motif for the RNA-binding proteins Pumilio 1 and 2 (Pum1/2) is underrepresented in transcriptomes of developing axons. Introduction of Pumilio-binding elements (PBEs) into mRNAs containing a β-actin zipcode prevented axonal localization and translation. Pum2 is restricted to the soma of developing neurons, and Pum2-knockdown or blocking its binding to

*Correspondence: uh2112@cumc.columbia.edu.

AUTHOR CONTRIBUTIONS

U.H. conceived the project, J.C.M. and U.H. designed the experiments, J.C.M. with L.K.R. and H.F.P. performed most experiments and data analyses. D.M.I. and F.P. designed, performed and analyzed the in vivo experiments. J.C.M. and U.H. wrote the manuscript.

DECLARATION OF INTERESTS

The authors declare no competing interests.

mRNA caused the appearance and translation of PBE-containing mRNAs in axons. Pum2-deficient neurons exhibited axonal growth and branching defects in vivo, and impaired axon regeneration in vitro. These results reveal that Pum2 shapes axonal transcriptomes by preventing the transport of PBE-containing mRNAs into axons and they identify somatic mRNAs retention as a mechanism for the temporal control of intra-axonal protein synthesis.

Graphical Abstract

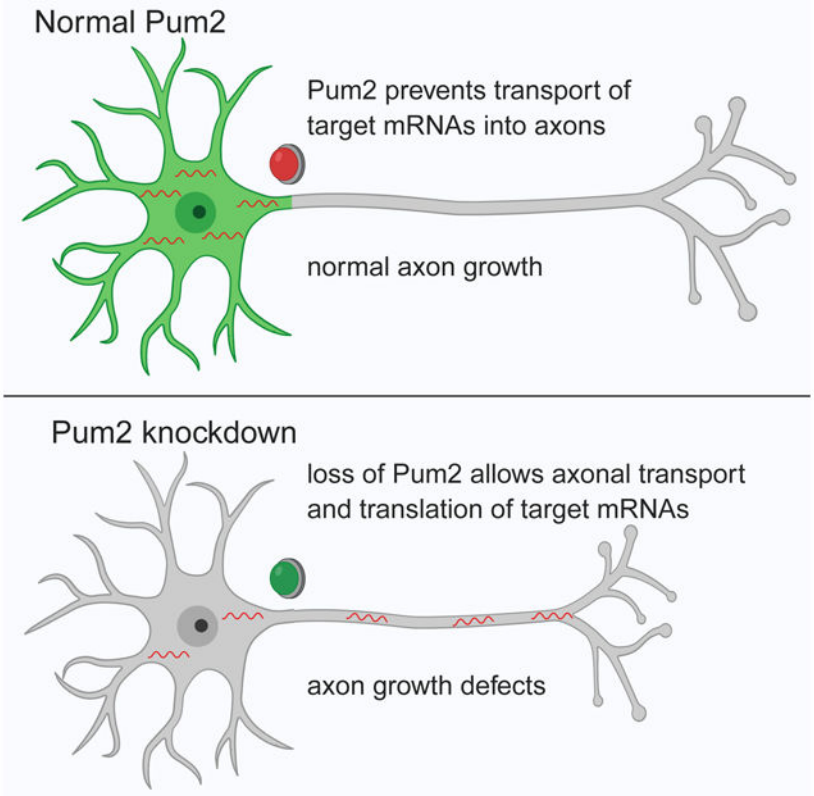

eTOC Blurb

Local translation of a specific subset of mRNAs in axons is critical for neuronal development. Martinez et al. report that the RNA-binding protein Pumilio 2 controls which transcripts are transported into axons by retaining its target mRNAs in the soma.

Keywords

Axonal transcriptome; zipcodes; Pumilio; axon development and regeneration; mRNA localization; local protein synthesis; locked nucleic acids

INTRODUCTION

Polarized cells rely on asymmetric mRNA translation to react acutely and in a spatially precise manner to changes in their environment. In neurons, local protein synthesis in axons is crucial for axon growth, branching, targeting, and maintenance (Holt and Schuman, 2013;

Jung et al., 2014). The current model for the subcellular localization of mRNAs in neurons involves primarily their incorporation into ribonucleoprotein particles (RNPs) which are actively transported into dendrites or axons (Kiebler and Bassell, 2006; Xing and Bassell, 2013). RNPs assemble through the association of RNA-binding proteins (RBPs) with mRNAs containing recognition motifs, usually found within their 3' untranslated regions (UTRs). The first of these zipcodes has been described in β-actin mRNA (Kislauskis et al., 1994) with more zipcodes having since been identified in axonally localized mRNAs including tau, GAP-43, COXIV or IMPA1 transcripts (Andreassi et al., 2010; Aronov et al., 1999; Aschrafi et al., 2010; Beckel-Mitchener et al., 2002). However, despite the availability of several high quality, RNA-sequencing derived axonal transcriptomes from various neurons and developmental stages (Baleriola et al., 2014; Briese et al., 2016; Minis et al., 2014), the cis-acting elements responsible for the axonal localization of most transcripts remain unknown.

Many RBPs have been identified in neurons but in many cases it is unknown whether they contribute to axonal mRNA localization. The Puf (Pumilio and FBF) family of RNA-binding proteins regulates mRNA expression and localization of target mRNAs (Quenault et al., 2011). Two Pumilio homologs (Pum1 and Pum2) have been identified in mammals (Spassov and Jurecic, 2002) that recognize and bind to a shared RNA motif, the Pumilio binding element (PBE) (Galgano et al., 2008; Hafner et al., 2010; Morris et al., 2008). Pumilios can inhibit translation and mRNA stability by recruiting specific factors to target mRNAs. Pumilios can regulate mRNA deadenylation by the recruitment of CPEB or the CCR4-Pop2-NOT complex (Campbell et al., 2012; Pique et al., 2008; Van Etten et al., 2012; Weidmann et al., 2014). Pumilio proteins are also predicted to interact with miRNAs; Pum1 represses the translation of p27 mRNA through the recruitment of miR-221/222 (Kedde et al., 2010). In progenitor cortical radial glial cells, Pum2 and Staufen-2 RNA granules are apically localized promoting self-renewal and preventing premature neuronal differentiation (Vessey et al., 2012), and Pum1 and Pum2 are critical for hippocampal neurogenesis and function (Zhang et al., 2017). Pum2 forms dendritically localized RNP and stress granules involved in regulating dendritic spines formation and synaptic plasticity (Siemen et al., 2011; Vessey et al., 2010; Vessey et al., 2006). Pum1 knockout mice develop motor dysfunction through neurodegenerative processes in the cerebellum caused by Ataxin-1 overexpression, and in humans Pum1 haploinsufficiency causes developmental delay and seizures (Gennarino et al., 2018; Gennarino et al., 2015).

Research in most major model systems has revealed a much richer repertoire of mechanisms for mRNA localization than just active transport directed by the interplay of zipcodes and cognate RBPs: asymmetric mRNA localization can be achieved through localized transcription, compartment-specific mRNA degradation and stabilization, or diffusion and anchoring (Shav-Tal and Singer, 2005). Currently, it is unclear to what extent these other mechanisms are relevant for the shaping of axonal transcriptomes.

Here, we used a bioinformatics approach to identify sequence elements that are asymmetrically distributed between axonal and somato-dendritic transcriptomes. We found that PBEs are underrepresented in axonal transcripts and act as a zipcode for the retention of mRNAs in the neuronal cell body. Disruption of this zipcode or its RBP, Pum2, leads to

erroneous localization of mRNAs in axons and axon growth and branching defects indicating that anchoring of mRNAs in the cell body of developing neurons is an important mechanism to prevent mislocalization of mRNAs to axons.

RESULTS

PBEs are negatively correlated with axonal mRNA localization in developing sensory neurons

To identify motifs that might be instructive for axonal mRNA localization we used an approach developed to find mutual information between sequence elements and biological properties of mRNAs (Goodarzi et al., 2012) that is based on a framework for Finding Informative Regulatory Elements (FIRE) (Elemento et al., 2007). This approach identifies sequence elements that are under- or overrepresented in different transcriptomes; we used the top 6,000 transcripts in the axonal and cell body transcriptome sets from mouse embryonic DRG neurons (Minis et al., 2014). We identified several motifs that are overrepresented in cell body localized mRNAs and underrepresented in the axonal transcriptome (Figure 1A). The most informative motif (UGUAAAU) closely resembles the PBE motif recognized by the mammalian Puf proteins Pum1 and Pum2 (UGUAHAUA; with H representing A, C, U, but not G) (Galgano et al., 2008; Morris et al., 2008; Wang et al., 2002; White et al., 2001). We used an orthogonal approach to identify motifs regulating axonal mRNA localization by applying the computational algorithm DRIMust (Leibovich et al., 2013) to the same datasets. This algorithm found no motifs when using axonally enriched mRNAs as target sequences but found two motifs when using somatically enriched mRNAs as target sequences, of which one (UGUWU; with W representing A or U) is included in the motif identified by FIRE (Figure 1B).

Pum1 and Pum2 recognize the same core motif, but Pum2 is more flexible in its nucleotide recognition at the eighth base with a consensus motif of UGUAHAUW (Zhang et al., 2017). We tested the contribution of this base to the mutual information content of the motif using FIRE and found that the Pum2 motif (A or U in eighth position) is slightly more informative, i.e. predictive for exclusion from the axonal transcriptome, than the Pum1/2 motif, although both were highly informative (Figure 1C). The fifth base of mammalian PBEs can be A, C, or U but not G. In a directed FIRE analysis using the PBE with all four nucleotides in the fifth position, only the U, C, and A motifs were significantly informative for somatic enrichment of the mRNAs (Figure 1C). Together, these analyses indicated that the presence of a PBE in an mRNA is negatively correlated with its axonal localization in developing DRGs.

PBEs are informative for mRNA localization across different neuronal cell types

To test whether the presence of a PBE is informative for axon versus cell body localization of mRNAs in other neurons or neuronal cells, we ran FIRE analyses on transcriptome datasets from the somatic and neuritic compartments of the mouse neuroblastoma cell line N2A and of primary mouse cortical neurons (Taliaferro et al., 2016). Like in DRG neurons, both motifs were overrepresented in the somatically localized mRNAs and underrepresented

in neuritically enriched mRNAs in N2A cells and in cortical neurons (Figure 1D,E). The Pum2 motif was slightly more informative than the Pum1/2 motif in both cell types.

The PBE is sufficient to decrease axonal mRNA localization and translation

The analyses so far suggested that the presence of PBEs prevents mRNA localization and translation in axons of developing neurons. In agreement with this observation we found that mRNAs that contained two or more PBEs in their 3'UTR had an overall higher somatic expression in the mouse DRG transcriptome (Figure 2A). We directly tested this hypothesis in DRG neurons by overexpressing a reporter transcript comprising an ORF for GFP followed by the 3' UTR of *Actb*. The reporter construct was delivered to the somatic compartment of DRG neurons cultured in microfluidic chambers and the presence of the reporter mRNA was subsequently measured in axons. The β-actin zipcode in the *Actb* 3'UTR of this construct is sufficient to drive axonal localization (Kislauskis et al., 1994). The insertion of two flanking functional PBEs (UGUAUAUA) but not of mutated PBEs (UGUAGAUA) was sufficient to significantly reduce the axonal localization of the reporter transcript while at the same time slightly increasing its abundance in neuronal cell bodies (Figure 2B). To assess whether the reporter constructs were translated in axons, we used puromycylation with proximity ligation assay (puro-PLA) (tom Dieck et al., 2015). The presence of PBEs decreased the axonal synthesis of GFP while mutated version of the PBE did not (Figure 2C).

Next, we investigated whether the presence of PBEs was sufficient to mediate binding of Pum2 to the reporter mRNAs. We co-expressed Pum2 and the reporter constructs in HEK293T cells and carried out RNA immunoprecipitation (RIP) with qPCR. Only the PBE-containing reporter transcripts co-immunoprecipitated specifically with Pum2 (Figure 2D). These findings indicate that PBEs, possibly due to Pum2 binding, are sufficient to decrease mRNA localization and in consequence translation in axons.

Pum1/2 are differentially expressed in neurons

The polarized distribution of PBE-containing mRNAs prompted us to investigate whether the mammalian Pumilios Pum1 and Pum2 exhibit a similarly polarized subcellular localization in neurons. Immunocytochemistry on rat embryonic primary DRG, cortical, and hippocampal neurons revealed that Pum1 is found throughout the developing neurons but enriched in the axons, while Pum2 expression is restricted to the soma of all neurons tested (Figure 3A). The differential expression of Pum1 and 2 might at least in part be due to local protein synthesis, especially as transcripts coding for Pum1 are part of the transcriptome found in developing axons (Minis et al., 2014). To directly test whether Pum1 or Pum2 are locally synthesized in DRG axons we used puro-PLA. Pum1 puro-PLA puncta were readily detectable in axons while only very few puncta for Pum2 were present (Figure 3B).

Developmental regulation of Pum1/2 mirrors axonal translation of PBE-containing mRNAs

By probing lysates of mouse cortices of different ages for Pum1 and 2, we found that Pum2 protein expression peaked during the embryonic stage and progressively declined during development, while Pum1 expression briefly peaked postnatally before declining (Figure 3C). This data is consistent with a recent finding that Pum1/2 are highly expressed during

neurogenesis where they have a regulatory role, and that expression of both Pum1/2 is decreased by P30 in mice (Zhang et al., 2017).

If Pum1 and Pum2 are required for restricting the axonal localization of PBE-containing mRNAs in developing neurons, one might expect to find those mRNAs localized and translated in fully mature axons when Pum1 and Pum2 expression are downregulated. To test whether the correlation of PBE presence and soma localization of mRNAs was developmentally regulated in parallel with Pum1/2 expression, we tested the mutual information content of PBEs using FIRE on Ribo-Seq data from developing mouse retinal axon in vivo across different developmental stages (Shigeoka et al., 2016). This dataset is enriched in translating mRNAs but evidence suggest that the local translatome and transcriptome are highly correlated in neurons (Zappulo et al., 2017). When focusing the analysis on the mRNAs translated in axons at different developmental stages (E17.5, P0.5, P7.5, and adult), the Pum2 motif was highly informative for axonal mRNA translation (and thus localization) at different developmental stages, specifically by being highly underrepresented in mRNAs that are translated early (E17.5, P0.5) and overrepresented in mRNAs that are translated late (P7.5 and adult) (Figure 3D).

Together, these data suggest that expression of Pumilios, especially Pum2, is required for the polarized localization of mRNAs in developing neurons.

Axonal localization of PBE-containing mRNAs is increased upon Pum2 knockdown

Based on our findings thus far, it is likely that both Pum1 and Pum2 play a role in shaping the axonal transcriptome of developing neurons. Due to the somatic localization of Pum2 and because the Pum2 motif was slightly more informative of somatic enrichment in all datasets analyzed, we chose to focus on the role of Pum2 in somatic retention of mRNAs. It is likely that Pum1 plays a parallel role that is not explored here, possibly in the translational repression or degradation of transcripts in the axon.

To further investigate the role of Pum2 in shaping the axonal and cell body transcriptomes, we cultured rat embryonic DRG neurons in microfluidic chambers and transduced them with viruses expressing non-targeting control or Pum2-targeting shRNAs (shControl or shPum2). Expression of shPum2 caused a nearly complete reduction of Pum2 expression without significantly affecting the levels of Pum1 (Figure 4A). Pum2 knockdown resulted in a significant increase in axonal mRNA levels of two Pum2 targets: *L1cam* and *Gsk3b*, while a transcript that is not targeted by Pum2, *RpL13*, was unchanged (Figure 4B). The 3'UTRs of both *L1cam* and *Gsk3β* contain multiple PBEs and binding of Pum2 to both targets has been confirmed by iCLIP (Zhang et al., 2017). Somatic levels of these transcripts were also unaffected, indicating that it was not a result of an overall change in transcript abundance (Figure 4C). To determine the specificity of this effect, we used a rescue strategy to re-express Pum2 in shPum2 neurons using a Pum2 construct that has a mutation in the shRNA target site (Pum2R). Expression of the Pum2R construct efficiently rescued levels of Pum2 (Figure 4D). We sought to determine whether Pum2 rescue could reverse the axonal localization phenotype we had observed, so we focused on *L1cam* which showed the largest increase in axons after Pum2 knockdown. Pum2 rescue returned the axonal levels of *L1cam*

mRNA near baseline (Figure 4E), while not affecting the non-target *Rpl13* or changing overall somatic levels of either transcript (Figure 4F).

Blockage of an endogenous PBE in L1cam mRNA increases its axonal localization

To determine if axonal localization could also be increased by preventing Pum2 binding to an endogenous target, we used a locked nucleic acid (LNA) oligomer designed to interfere with Pumilio binding to the PBE in the Pum2 target *L1cam*. LNAs are modified RNA nucleotides that bind RNAs with high specificity thereby blocking binding of RNA-binding proteins (Koshkin et al., 1998; Villarin et al., 2016). *L1cam* was selected because its localization is significantly increased in axons with Pum2 knockdown (Figure 4B) and because its 3'UTR contains only two PBEs. We designed an LNA oligonucleotide to target the PBE closest to the *L1cam* coding sequence (Figure 4G) because regulatory elements proximal to the coding sequence can have the strongest regulatory effect (Kandasamy et al., 2005). Transfection of DRG cell bodies but not of their axons with LNAs targeting the *L1cam* PBE significantly increased the levels of *L1cam* mRNA in axons compared to a non-targeting control LNA, while *Gsk3b*, which contains several PBEs but was not targeted by the LNA, was unaffected (Figure 4H). Overall levels of somatic *L1cam* and *Gsk3b* were unchanged, and *Pum2* levels were also unaffected, indicating that the effects were not due to changes in Pum2 expression (Figure 4I).

Pum2 knockdown selectively changes axonal transcriptome composition without altering overall neuronal mRNA levels

Next, we analyzed the effects of Pum2 knockdown on mRNA localization on a transcriptome-wide level by sequencing the cell body and axonal transcriptomes of DRG neurons transduced with shControl or shPum2 viruses. First, we compared the newly generated axonal transcriptome of shControl expressing DRGs to the previously published mouse axonal transcriptome (Minis et al., 2014) and found over 70% overlap of the top expressed genes (Figure 5A). Gene Ontology analysis generated distinct term lists for axonal and somatically enriched transcripts with developmental programs being more prominent in the cell bodies and translation and mitochondrial processes in axons (Figure 5B). Directed FIRE analysis in non-discovery mode revealed that the Pum2 and Pum1/2 motifs were overrepresented in somatically localized mRNAs and underrepresented in axonal mRNAs as expected (Figure 5C). Additionally, similarly to the mouse DRG transcriptome (Figure 2A), we found that mRNAs containing at least one or more PBEs were more highly expressed in the somatic compartment (Figure 5D). Since it has been reported that Pum1/2 can regulate mRNA stability, we analyzed whether knocking down Pum2 would result in major changes of the cell body transcriptome. Using differential gene expression analysis on the somatic transcriptomes, we found that knocking down Pum2 did not result in any significant changes in overall mRNA expression except for Pum2 itself (Figure 5E). On the contrary, differential gene expression analysis of the axonal transcriptomes revealed that Pum2 knockdown resulted in deregulation of axonal localization of many mRNAs. Interestingly, there was a much bigger increase of mRNAs in axons in the shPum2 condition while the overall distribution of mRNAs based on the number of PBEs remains similar across both conditions (Figure 5F). Together, these findings suggest that Pum2 regulates axonal mRNA content without regulating mRNA stability in neuronal cell bodies.

mRNA localization of PBE-containing mRNAs in axons is increased by Pum2 knockdown

Next, we focused on the axonal transcriptome changes upon Pum2 knockdown. Specifically, we analyzed the mutual information content of the PBE across axonal mRNA expression of shControl versus shPum2 transduced neurons. The PBE was highly underrepresented in mRNAs whose localization did not change across conditions, while it was overrepresented in mRNAs that became enriched in axons after the knockdown (Figure 6A). We also tested this effect by directly comparing the group of mRNAs that was upregulated in axons after Pum2 knockdown to the group of mRNAs that was unchanged using FIRE in binary mode and observed a strong over-representation of the PBE in the set of mRNAs that was localized to axons upon knockdown (Figure 6B). Similarly, comparing the ten most strongly up- and downregulated mRNAs in axons of *Pum2*-deficient neurons revealed that a larger proportion (5/10) of the upregulated transcripts contained a PBE while most downregulated did not (8/10) (Table 1). As Pum2 has many targets including other RNA-binding proteins, it is possible that up- or downregulated transcripts lacking a PBE are the result of secondary effects of Pum2 knockdown. Gene ontology analysis revealed distinct terms for the up- or downregulated mRNAs in axons of shPum2 expressing DRG neurons (Figure 6C).

Pum2 knockdown increases overall translation levels in axons

Since Pum2 downregulation leads to an increase of PBE-containing mRNAs in axons, we hypothesize that overall axonal translation might be affected. We quantified axonal protein synthesis in DRG neuron axons by measuring the amount of puromycin incorporation during a 10-minute labeling period. Expression of shPum2 caused an increase in total axonal protein synthesis of around 30% (Figure 6D).

Pum2 knockdown increases axonal translation of a specific target, Gsk3b

To test whether this overall increase in axonal translation included the translation of specific PBE-containing mRNAs, we carried out a puro-PLA assay for a putative Pum2-target mRNA, *Gsk3b*. This mRNA was significantly increased in axons upon Pum2 knockdown (Figure 4B). Puro-PLA for GSK3β revealed a significant increase in the translation of *Gsk3b* in axons of *Pum2*-deficient DRG neurons (Figure 6E), and this increased synthesis was reflected in significantly increased levels of GSK3β in axons (Figure 6F).

Downregulation of Pum2 in vivo results in impaired contralateral axon outgrowth and branching

To determine whether the changes in mRNA localization upon Pum2 knockdown would affect axon development in vivo, we delivered shRNAs to neural progenitors layer 2/3 pyramidal neurons (PNs) projecting to the contralateral cortex (callosal projections) by in utero electroporation (Courchet et al., 2013; Hand and Polleux, 2011). In mice, axons of these neurons cross the cortical midline around birth, reach the contralateral cortex during the first postnatal week and branch into layers 2/3 and 5 between P8 and P15 (Courchet et al., 2013). We electroporated constructs driving the expression of control shRNA (shControl) or shRNA targeting Pum2 (shPum2) and ZsGreen into one hemisphere of the cortex of mouse embryos at E15.5, at which time Pum2 expression is high. At P5 or P21 the mouse brains were sectioned and midline crossing or contralateral axon growth/branching,

respectively, were measured (Figure 7A). At P5, while these axons have crossed the midline and still grow towards their contralateral target, we detected a significant reduction in the ratio of post- over pre-crossing GFP-positive axons at the midline in the shPum2 condition compared to shControl suggesting that Pum2 is involved in early axon extension (Figure 7B). At P21, when the axons had reached their adult-like pattern of branching contralaterally, we measured axon branching by normalizing the GFP fluorescence intensity throughout cortical layers to the intensity of GFP-positive axons in the white matter in order to account for potential differences in numbers of electroporated axons reaching the contralateral cortex (Courchet et al., 2013). Knocking down Pum2 caused a significant decrease in axon branching both in layers 2/3 and layer 5 in the contralateral cortex compared to control (Figure 7C). Therefore, Pum2 is required for proper cortical axon growth and branching during neuronal development in vivo, and its depletion early in development has long-lasting effects.

Pum2 disruption results in impaired axon regeneration after injury

Axonal mRNA localization and translation are tightly regulated in response to nerve injury to establish an appropriate axon regeneration program (Terenzio et al., 2018; Zheng et al., 2001). To test whether disrupting this pathway would influence axon regeneration we knocked down Pum2 expression in DRG neurons grown in microfluidic chambers and severed their axons by aspiration of the axonal compartment. 24 hours later, axon regrowth was significantly reduced in the shPum2 condition, and this phenotype was partially rescued by expression of a shRNA-resistant Pum2 construct (Figure 7D), revealing that Pum2 knockdown interferes with axonal regeneration.

Together, our results establish a novel mechanism for the regulation of mRNA localization in developing axons: mRNAs containing a PBE are prevented from localizing to axons by their Pum2-dependent retention in the cell bodies and the disruption of this localization mechanism causes defects in axon development and regeneration.

DISCUSSION

A critical gap in our understanding of local protein synthesis in neurons is the incomplete knowledge of the full complement of cis- and trans-acting factors that regulate localization of mRNAs to various cellular compartments. Research has mostly focused on the handful of identified sequence elements that drive the axonal localization of the relatively few mRNAs containing these zipcodes. Despite the availability of axonal transcriptome and translatome data sets, the identification of additional zipcodes has been unexpectedly challenging, leading to the question of whether other localization mechanisms might exist, such as have been described in other model organisms. In fact, a gating mechanism that restricts the localization of mRNAs into axons had been discussed but so far not been found in neurons (Jung et al., 2012). Here, we identified the PBE as a retention element that strongly restricts localization of mRNAs to the soma. This finding expands the repertoire of known mechanisms for the subcellular localization of mRNAs in neurons. In our computational analysis we did not find any ‘positive’ localizing elements. This might be caused by limiting our search to short sequences elements (7 nucleotides versus 54 for the β-actin zipcode). A

surprising aspect of our study is that at least in developing neurons Pum1 and Pum2 are not functionally redundant. An analysis of Pum1 and Pum2 associated mRNAs in HeLa cells demonstrated partially overlapping target sets (Galgano et al., 2008), and the fact that Pum2-deficient mice are fertile and viable further supported the notion that Pum1 and 2 are functionally redundant at least in reproductive organs (Xu et al., 2007). In contrast, we find distinct subcellular localization patterns for Pum1 and Pum2 in developing neurons. This result is consistent with a prior finding showing that in the mouse neuromuscular junction Pum1 is localized pre-synaptically, while Pum2 is localized post-synaptically (Marrero et al., 2011). Further supporting distinct functions for the Pumilios is our finding that knockdown of Pum2 leads to mislocalization of mRNAs to axons and axon branching defects that are not compensated for by Pum1. The function of Pum1 in developing axons remains unknown but it might act in concert with Pum2 by regulating the expression of PBE-containing mRNAs that escaped the Pum2-mediated retention in the soma.

We identified Pum2 as a regulator of axonal mRNA localization in developing neurons. In agreement with a recent study (Zhang et al., 2017), we found that Pum2 does not globally affect mRNA levels in neurons. Instead, Pum2-mediated mRNA localization is likely a consequence of Pum2's exclusive expression in the somatic compartment of neurons, and not due to the control of mRNA stability as proposed in other systems (Burow et al., 2015). We found that the expression of Pum2 in the brain is developmentally regulated with highest levels coinciding with axon growth and pathfinding. This developmental regulation of Pum2 is mirrored in the appearance of PBE-containing mRNAs in the transcriptome of mature axons (Shigeoka et al., 2016), suggesting a mechanism for the stage-dependent control of axonal translation. The Pum2-dependent retention of mRNAs in the neuronal soma might shape the axonal transcriptome such that it supports axon growth and development, while the developmental downregulation of Pum2 leads to a reshaping of the axonal transcriptome supporting the post-developmental maintenance of axons. In line with this idea, we observed that the knockdown of Pum2 interferes with axon growth and branching in the cortex and regeneration of severed DRG axons. One of the mRNAs that are kept out of axons by Pum2 is *Gsk3b*. Inhibition of GSK3β is crucial for axonal development (Kim et al., 2011) and axonal GSK3β activity and mTORC1 activities are precisely balanced to support axon regeneration (Miao et al., 2016). mTOR activity is strongly linked to the regulation of axonal protein synthesis (Campbell and Holt, 2001) and axonal branching and regeneration (Spillane et al., 2013; Terenzio et al., 2018). Shigeoka et al. (2016) found that the translation of mTORC1 targets in axons peaks at P0.5, the stage of axon wiring. We found the highest repression of Pum2 targets in axons at this stage. Thus, Pum2 might at least in part act by preventing the synthesis of proteins that would counter mTOR-dependent local translation required for axon development and regeneration.

In conclusion, we describe a mechanism for the control of axonal mRNA localization and translation. The presence of PBE acts as an anti-zipcode in developing neurons through the Pum2-dependent retention of transcripts in the neuronal cell body. Our results provide a mechanism for the temporal control of axonal translatome composition.

STAR METHODS

LEAD CONTACT AND MATERIALS AVAILABILITY

Further information and requests for resources and reagents should be directed to and will be fulfilled by the Lead Contact, Ulrich Hengst (uh2112@cumc.columbia.edu)

EXPERIMENTAL MODEL AND SUBJECT DETAILS

Primary neuron culture—Pregnant Sprague-Dawley rats *(Rattus norvegicus)* were obtained from Envigo (Indianapolis, IN) and single-housed for 2 days at the barrier facility at the Columbia University Institute of Comparative Medicine. All rodent procedures were approved by the Columbia University Institutional Animal Care and Use Committee. Rats were euthanized by gas displacement with 5% min^{-1} CO_2 until there were no signs of breathing, approximately 6-7 min. A secondary physical means of euthanasia, bilateral thoracotomy, was performed to ensure death. DRGs were harvested from E14 rat embryos of both sexes and trypsinized by incubating with TrypLE Express for 30 min in a water bath at 37°C. DRGs were centrifuged to remove TrypLE solution. They were washed once with DRG growth medium (Neurobasal, l×B27, 2 mM glutamate, 20 μM 5-FdU, 50 ng ml^{-1} NGF) and resuspended in the same media and dissociated with a fine pipette tip. About 30,000 cells were seeded per chamber and allowed to attach for 30 mins before more medium was added. For Puro-PLA experiments glass bottom dishes (MatTek, Ashland, MA) were coated with 0.1 mg ml^{-1} PLL (Trevigen, Gaithersburg, MD) for 1 h at 37°C and then rinsed with water three times and allowed to air-dry. For the rest of the experiments glass coverslips (25 mm; Carolina Biological Supply Company, Burlington, NC) were rinsed with water twice and then coated with PLL in a 6-well Nunc cell-culture treated 6-well plate for 1 h at 37°C. Coverslips were then rinsed with water three times and allowed to air-dry. Cells were maintained at 37°C with 5% CO_2 for up to one week with full medium changes every 2-3 days.

Mice—All animals were handled according to protocols approved by the Institutional Animal Care and Use Committee at Columbia University, New York. Mice used for *in utero* electroporation were F1 wild-type mice from a cross of **C57BL/6J and 129S1/SvImJ** backgrounds. Timed-pregnant female mice were maintained in a 12 hour light/dark cycle and obtained by overnight breeding with males of the same strain. For timed-pregnant mating, noon after mating is considered E0.5.

METHOD DETAILS

Compartmentalized cultures—Bipartite microfluidic devices with a set of 750 μm-long microgroove barriers were designed in house and master molds were produced according to established protocol (Park et al., 2006; Taylor et al., 2005). Briefly, 4-inch silicon wafers (UniversityWafer, Boston, MA) were coated with SU-8 5 (MicroChem Corp, Westborough, MA) on a spin coater at 3,000 rpm for 60 seconds. Coated wafers were baked for 2 minutes at 95°C on a hotplate and then exposed to UV light (100 mJ cm^{-2}, constant dose) through a transparency mask (Front Range PhotoMask, Lake Havasu City, AZ) containing the microgrooves pattern. Wafers were baked again for 2 minutes at 95°C on a hotplate, then non-crosslinked SU-8 was removed by immersion in propylene glycol methyl ether acetate

(PGMEA) for 3 minutes with constant agitation. Wafers were dried with pressurized nitrogen and coated with SU-8 2050 (MicroChem Corp, Westborough, MA) on a spin coater at 1,500 rpm for 60 seconds. Coated wafers were baked for 3 minutes at 65°C, then 9 minutes at 95°C on a hotplate, then exposed to UV light (230 mJ cm^{-2}, constant dose) through a transparency mask containing the chamber pattern. Wafers were baked again for 5 minutes at 65°C, then 12 minutes at 95°C on a hotplate, then non-crosslinked SU-8 was removed by immersion in PGMEA for 15 minutes with constant agitation. Finished master molds were washed with fresh PGMEA followed by isopropanol and dried with pressurized nitrogen. Molds were then hard baked for 5 minutes at 150°C. This work was performed in a cleanroom at the Advanced Science Research Center NanoFabrication Facility of the Graduate Center at the City University of New York. For a detailed protocol, see Birdsall et al. (2019). Microfluidic chambers were produced from master molds using PDMS (Sylgard 184, or QSil 216) by combining an elastomer base with curing agent in a 10:1 ratio and mixing thoroughly for 5-15 mins. Trapped gases were removed by placing the mixture in a vacuum desiccator for 1-2 h. PDMS molds were baked for at 4 h at 65°C. Individual devices were cut and reservoir holes were punched. Chambers were cleaned with vinyl tape, washed in 70% ethanol and dried before use.

DNA constructs—Lentivirus expression plasmids with shRNAs targeting Pum2 or control sequence targeting the SV40 promoter (shPum2 sequence: tgctgttgacagtgagcgCGCGAATAAACCACTTGTTGAA-tagtgaagccacagatgtaTTCAACAAGTGGTTTATTCGCTtgcctactgcctcgga; shControl sequence: tgctgttgacagtgagcgAAGGCAGAAGTATGCAAAGCATtagtgaagccacagatgtaATGCTTT-GCATACTTCTGCCTGtgcctactgcctcgga; capital letters indicate gene-targeting hairpin sequence) were obtained from transOMIC (Huntsville, AL). The hairpins in these plasmids are designed using algorithms and technology that enhances specificity and potency (Auyeung et al., 2013; Knott et al., 2014). These plasmids were slightly altered by replacing the original mCMV promoter with the hUbC promoter for better expression in primary neurons using the In-Fusion HD Cloning Plus kit (Takara Bio, Mountain View, CA). Also, the reporter ZsGreen1 gene and Puromycin resistance cassette were replaced by eGFP. For expression of Pum2 or shRNA-resistant Pum2, the lentiviral FUGW plasmid (Lois et al., 2002) was modified by In-Fusion cloning to replace GFP with the mouse Pum2 coding sequence or mouse Pum2 containing a single-nucleotide synonymous mutation of proline 210 (CCA to CCG) in the shRNA-targeting site, respectively. For expression of GFP reporter constructs, the FUGW plasmid was modified by adding the first 400 bp of the mouse *Actb* 3'UTR after GFP with or without two flanking Pumilio binding elements (UGUAUAUA) or mutated Pumilio binding elements (UGUAGAUA).

Lentivirus preparation—Lentiviruses are produced by transfecting HEK293T cells with the lentiviral plasmid and packaging plasmids (pCMVΔ R8.9 and pHCMV VSVg) (Lois et al., 2002) using Calfectin (Signagen, Rockville, MD). Medium is changed to DRG growth medium without NGF or FdU after 8h. Viruses are collected 24h later, aliquoted and stored at −80°C. The titers for every batch are calculated using a qPCR-based kit from Applied Biological Materials (Richmond, Canada) according to the manufacturer's instructions.

Primary DRG neurons were infected 30 mins after plating at an MOI of 10 for shRNA viruses and MOI of 1 for Pum2 rescue virus to obtain more than 90% infectivity. Knockdown and rescue were measured 4-7 days after infection.

LNA transfection—LNAs were transfected at a final concentration of 100 nM into the cell body or axonal compartment on DIV5 using NeuroPORTER (Genlantis, San Diego, CA) according to manufacturer's instructions. The following LNAs (Integrated DNA Technologies, Coralville, IA) were used to target bases 4748-4765 of rat *L1cam* mRNA (NM_017345): 5'-AC+GGT+GTA+TTT+ACA+TTC+C-3' and non-targeting control: 5'-GA+CTA+TAC+GCG+CAA+TAT+G-3'. Preposed + signifies LNA base. RNA was collected 48 hours after transfection.

In utero electroporation—In utero cortical electroporation was performed according to previously described protocols (Courchet et al., 2013; Hand and Polleux, 2011). Briefly, endotoxin-free DNA was injected using a glass pipette into one ventricle of the mouse embryos. The volume of injected DNA was adjusted depending on the experiments. Electroporation was performed at E15.5 using a square wave electroporator (ECM 830, BTX) and gold paddles. The electroporation settings were: 5 pulses of 45 V for 50 ms with 500 ms intervals. shPumilo2-GFP or shControl-GFP plasmids were used at 0.9 μg μl^{-1} for axon branching experiments at P21 and 1.2 μg μl^{-1} for midline crossing experiments at P5. Animals were perfused 5 days or 3 weeks after with 4% paraformaldehyde.

Axon growth and branching in vivo—Animals at the indicated age were anaesthetized with isofluorane before intracardiac perfusion with PBS and 4% PFA (Electron Microscopy Sciences). 100 μm coronal brain sections were obtained using a vibrating microtome (Leica VT1200S). Sections were mounted on slides in Fluoromount-G (SouthernBiotech). Confocal images of electroporated neurons in slices were acquired in 1024×1024 mode using an A1R laser scanning 11 confocal microscope controlled by the Nikon software NIS-Elements (Nikon Corporation, Melville, NY). We used a 10X H-TIRF, NA 0.45 (Nikon) objective lens to acquire image volumes of neuron fragments. All quantifications were performed in layer 2/3 of the primary somatosensory cortex in sections of comparable rostro-caudal position. To quantify contralateral axon branching at P21, pixel intensity measurements were obtained in NIS-Elements from contralateral cortical columns identified from maximum-intensity projection images (N = 21 cortical columns from 5 mice in the control condition; 18 cortical columns from 6 mice in the shPumilio2 condition). To quantify midline axon crossing at P5, pixel intensity measurements of post-crossing and pre-crossing regions of interest were obtained in NIS-Elements from maximum-intensity projection images (N = 15 tissue sections from 5 mice in the control condition; 13 tissue sections from 4 mice in the shPumilio2 condition).

Immunofluorescence—Primary DRG neurons were fixed with 4% paraformaldehyde in cytoskeletal preservation buffer (10 mM MES, 138 mM KCl, 3 mM $MgCl_2$, 2 mM EGTA, 320 mM sucrose, pH 6.1) for 15 minutes at room temperature. Samples were washed with PBS (3 times for 5 minutes each) and permeabilized in PBS with 0.3% Triton X-100 for 5 minutes. Cells were rinsed briefly in PBS and blocked for 1 h at room temperature with 5%

BSA in PBS-T (0.1% Tween-20 in 1X PBS). Samples were incubated overnight in 1% BSA in PBS-T at 4°C with the following primary antibodies: β-III-tubulin (1:1,000, BioLegend), Pum1 (1:200, Bethyl), Pum2 (1:200, Bethyl), GSK-3β (1:100, Cell Signaling). Samples were washed with PBS-T (3 times, 5 minutes each) and incubated for 1 hour at room temperature with fluorophore-conjugated Alexa secondary antibodies (1:1,000, Thermo Fisher Scientific) and/or fluorescence conjugated β-III-tubulin (1:500, BioLegend). Samples were washed with PBS (3 times, 5 minutes each), and mounted with ProLong Diamond antifade reagent (Thermo Fisher Scientific). Imaging was carried out using an EC Plan-Neofluar 40×/1.3 objective on an Axio-Observer.Z1 microscope equipped with an AxioCam MRm Rev. 3 camera or on an LSM 800 confocal microscope (Zeiss, Thornwood, NY).

Puromycylation—Primary DRG neurons grown in microfluidic devices were incubated with 2 μM puromycin (Thermo Fisher Scientific) only in the axonal compartment at 37°C for 10 minutes. Cells were washed once with fresh DRG growth medium and then fixed and processed as described above for immunocytochemistry with the following modifications. Samples were incubated overnight at 4°C with anti-puromycin antibody (1:1,000, Millipore Sigma) and the next day with fluorescence conjugated β-III-tubulin (1:500, BioLegend) and Alexa-conjugated secondary for 1 h at room temperature.

Puro-PLA—Puro-PLA assay to detect newly synthesized proteins following an established protocol (tom Dieck et al., 2015). Briefly, the puromycylation procedure detailed above was combined with the Duolink (Sigma-Aldrich) assay according to the manufacturer's instructions as follows. Fixed cells were incubated overnight at 4°C with anti-puromycin antibody (1:1,000, Millipore Sigma) in addition to antibodies against the following proteins of interest: GFP (1:1500, Thermo Fisher Scientific), GSK-3β (1:100, Cell Signaling). After primary antibody incubation and washes, samples were incubated with Plus and Minus conjugated PLA probes for 1h at 37°C in humidity chambers. Samples were then washed twice in TBS-T for 5 minutes each time. Ligation of the probes was carried out for 30 mins at 37°C and followed with 2 washes for 2 minutes with TBS-T. Amplification using the red reagent mix was performed for 100 mins at 37°C. Samples were washed with TBS and incubated with fluorescence conjugated β-III-tubulin (1:500, BioLegend) in TBS for 1 h at room temperature. Finally, samples were rinsed in TBS and mounted using Duolink Mounting Media with DAPI (Sigma-Aldrich).

Quantitative Real Time PCR—Total RNA was extracted from either the somatic or axonal compartment using the Single Cell RNA Purification Kit (Norgen Biotek, Thorold, ON, Canada) from 6 chambers for soma or 12-20 chambers for axons. Samples were treated with DNAseI. Quantitative PCR was performed with the One-Step RT-qPCR from RNA kit (Bio-Rad) according to manufacturer's instructions using gene-specific TaqMan probes. 10 ng of somatic RNA was used per reaction. Axonal RNA was too low to measure therefore loading was normalized to volume and results were normalized to a reference gene. After performing RT-PCR (iScript RT Supermix, Bio-Rad), axonal samples were preamplified (SsoAdvanced PreAmp Supermix, Bio-Rad) and qPCR was subsequently performed with SsoAdvanced Universal Probes Supermix (Bio-Rad).

RNA-sequencing—Total RNA was extracted from either the somatic or axonal compartment using the Single Cell RNA Purification Kit (Norgen Biotek, Thorold, ON, Canada) from 6 microfluidic chambers. Samples were submitted to GENEWIZ for RNA-Seq. mRNA was enriched by poly-A pulldown. Axonal RNA was subjected to SMART-Seq v4 Ultra Low Input RNA Kit while somatic RNA library was prepared using a standard mRNA kit. Generated libraries were pooled together and sequenced using a HiSeq 2×l50bp PE configuration in a single high output lane.

Motif Discovery and Testing—Motif discovery and analysis was performed using FIRE (Elemento et al., 2007) with a few modifications. Full length annotated 3'UTRs were downloaded from UCSC database using Usegalaxy Webserver. Duplicates were removed and sequence homology files were prepared using scripts included in the FIRE suite. Data files containing either continuous or discrete information were prepared from the RNA-Seq analysis and provided to the program accordingly. Since the sequencing was not deep enough to accurately measure transcript isoform expression and 3'UTRs are generally under-annotated, the isoforms containing the longest 3'UTR were often used in the analysis when multiple isoforms exist. The number of bins were set to result in 200 genes per bin. For de novo motif discovery analysis minr was set at 1.

QUANTIFICATION AND STATISTICAL ANALYSIS

General statistical analysis—Statistical analysis was performed using GraphPad Prism 8 software (GraphPad Software, Inc; La Jolla, CA). When comparing the means of two groups, a paired or unpaired *t*-test was performed depending on experimental design (see figure legends). When comparing the means of three independent groups, a one-way analysis of variance (ANOVA) with Dunnett's multiple comparisons test was performed. When comparing the means of multiple groups encompassing two independent variables, two-way ANOVA with Bonferroni's or Holm-Sidak multiple comparisons test was performed.

Image quantification—Immunofluorescence experiments were quantified using AxioVision software (Zeiss). A region of interest (ROI; total axonal area) was demarked in the counterstaining channel using β-III-tubulin staining to label axons. Average pixel intensity within the ROI was measured in all channels. Background pixel intensity was calculated in an area outside the ROI and subtracted from the measurements. Puro-PLA experiments were quantified using Fiji (Schindelin et al., 2012). Axonal area was demarked as described above. PLA puncta within the ROI were counted manually and this number was divided by ROI area.

RNA-sequencing Analysis—Publicly available datasets were accessed and downloaded from the NCBI GEO database web server. Reads were pseudoaligned to that appropriate species transcriptome (mouse or rat) using kallisto under default conditions to generate transcript specific counts (Bray et al., 2016). For differential gene expression analysis, transcript counts were imported in R using tximport (Soneson et al., 2015) and analysis was performed with DESeq2 (Love et al., 2014). Generally, a stringent threshold was set to filter

lowly expressed genes from downstream analysis by excluding genes whose expression level were under the 75th quartile.

DATA AND CODE AVAILABILITY

The RNA sequencing data have been deposited in the GEO database (accession number: GSE135073).

ACKNOWLEDGMENTS

We thank Jamie Yang and Saeed Tavazoie for their helpful suggestions on the use of FIRE. J.C.M. was supported by the National Institute of General Medical Sciences (F31GM116617), L.K.R. was supported by training grants from the Eunice Kennedy Shriver National Institute of Child Health and Human Development and the National Institute of Neurological Disorders and Stroke (T32HD007430; T32NS064928), D.M.I was supported by the National Institute of Neurological Disorders and Stroke (T32NS064928; F31NS101820), H.F.P. was supported by the Ludwig-Maximilians-University (PROSA Scholarship) and the German Society of Neurology (Felgenhauer Prize), F.P. was supported by the National Institute of Neurological Disorders and Stroke (R01NS089456) and an award from the Fondation Roger De Spoelberch. U.H. was supported by grants from the National Institute of Mental Health (R01MH096702), the New York State Department of Health Spinal Cord Injury Research Board (C32089), and the Irma T. Hirschl Trust.

REFERENCES

Andreassi C, Zimmermann C, Mitter R, Fusco S, De Vita S, Saiardi A, and Riccio A (2010). An NGF-responsive element targets myo-inositol monophosphatase-1 mRNA to sympathetic neuron axons. Nat. Neurosci. 13, 291–301. [PubMed: 20118926]

Aronov S, Marx R, and Ginzburg I (1999). Identification of 3'UTR region implicated in tau mRNA stabilization in neuronal cells. J. Mol. Neurosci. 12, 131–145. [PubMed: 10527457]

Aschrafi A, Natera-Naranjo O, Gioio AE, and Kaplan BB (2010). Regulation of axonal trafficking of cytochrome c oxidase IV mRNA. Mol. Cell. Neurosci. 43, 422–430. [PubMed: 20144716]

Auyeung VC, Ulitsky I, McGeary SE, and Bartel DP (2013). Beyond secondary structure: primary-sequence determinants license pri-miRNA hairpins for processing. Cell 152, 844–858. [PubMed: 23415231]

Baleriola J, Walker CA, Jean YY, Crary JF, Troy CM, Nagy PL, and Hengst U (2014). Axonally synthesized ATF4 transmits a neurodegenerative signal across brain regions. Cell 158, 1159–1172. [PubMed: 25171414]

Beckel-Mitchener AC, Miera A, Keller R, and Perrone-Bizzozero NI (2002). Poly(A) tail length-dependent stabilization of GAP-43 mRNA by the RNA-binding protein HuD. J. Biol. Chem. 277, 27996–28002. [PubMed: 12034726]

Birdsall V, Martinez JC, Randolph L, Hengst U, and Waites CL (2019). Live Imaging of ESCRT Proteins in Microfluidically Isolated Hippocampal Axons. Methods Mol. Biol. 1998, 117–128. [PubMed: 31250298]

Bray NL, Pimentel H, Melsted P, and Pachter L (2016). Near-optimal probabilistic RNA-seq quantification. Nat. Biotechnol. 34, 525–527. [PubMed: 27043002]

Briese M, Saal L, Appenzeller S, Moradi M, Baluapuri A, and Sendtner M (2016). Whole transcriptome profiling reveals the RNA content of motor axons. Nucleic Acids Res. 44, e33. [PubMed: 26464439]

Burow DA, Umeh-Garcia MC, True MB, Bakhaj CD, Ardell DH, and Cleary MD (2015). Dynamic regulation of mRNA decay during neural development. Neural Dev. 10, 11. [PubMed: 25896902]

Campbell DS, and Holt CE (2001). Chemotropic responses of retinal growth cones mediated by rapid local protein synthesis and degradation. Neuron 32, 1013–1026. [PubMed: 11754834]

Campbell ZT, Menichelli E, Friend K, Wu J, Kimble J, Williamson JR, and Wickens M (2012). Identification of a conserved interface between PUF and CPEB proteins. J. Biol. Chem. 287, 18854–18862. [PubMed: 22496444]

Courchet J, Lewis TL Jr., Lee S, Courchet V, Liou DY, Aizawa S, and Polleux F (2013). Terminal axon branching is regulated by the LKB1-NUAK1 kinase pathway via presynaptic mitochondrial capture. Cell 153, 1510–1525. [PubMed: 23791179]

Elemento O, Slonim N, and Tavazoie S (2007). A universal framework for regulatory element discovery across all genomes and data types. Mol. Cell 28, 337–350. [PubMed: 17964271]

Galgano A, Forrer M, Jaskiewicz L, Kanitz A, Zavolan M, and Gerber AP (2008). Comparative analysis of mRNA targets for human PUF-family proteins suggests extensive interaction with the miRNA regulatory system. PLoS One 3, e3164. [PubMed: 18776931]

Gennarino VA, Palmer EE, McDonell LM, Wang L, Adamski CJ, Koire A, See L, Chen CA, Schaaf CP, Rosenfeld JA, et al. (2018). A Mild PUM1 Mutation Is Associated with Adult-Onset Ataxia, whereas Haploinsufficiency Causes Developmental Delay and Seizures. Cell 172, 924–936 e911. [PubMed: 29474920]

Gennarino VA, Singh RK, White JJ, De Maio A, Han K, Kim JY, Jafar-Nejad P, di Ronza A, Kang H, Sayegh LS, et al. (2015). Pumilio1 haploinsufficiency leads to SCA1-like neurodegeneration by increasing wild-type Ataxin1 levels. Cell 160, 1087–1098. [PubMed: 25768905]

Goodarzi H, Najafabadi HS, Oikonomou P, Greco TM, Fish L, Salavati R, Cristea IM, and Tavazoie S (2012). Systematic discovery of structural elements governing stability of mammalian messenger RNAs. Nature 485, 264–268. [PubMed: 22495308]

Hafner M, Landthaler M, Burger L, Khorshid M, Hausser J, Berninger P, Rothballer A, Ascano M Jr., Jungkamp AC, Munschauer M, et al. (2010). Transcriptome-wide identification of RNA-binding protein and microRNA target sites by PAR-CLIP. Cell 141, 129–141. [PubMed: 20371350]

Hand R, and Polleux F (2011). Neurogenin2 regulates the initial axon guidance of cortical pyramidal neurons projecting medially to the corpus callosum. Neural Dev. 6, 30. [PubMed: 21864333]

Holt CE, and Schuman EM (2013). The central dogma decentralized: new perspectives on RNA function and local translation in neurons. Neuron 80, 648–657. [PubMed: 24183017]

Jung H, Gkogkas CG, Sonenberg N, and Holt CE (2014). Remote control of gene function by local translation. Cell 157, 26–40. [PubMed: 24679524]

Jung H, Yoon BC, and Holt CE (2012). Axonal mRNA localization and local protein synthesis in nervous system assembly, maintenance and repair. Nat. Rev. Neurosci. 13, 308–324. [PubMed: 22498899]

Kandasamy K, Joseph K, Subramaniam K, Raymond JR, and Tholanikunnel BG (2005). Translational control of beta2-adrenergic receptor mRNA by T-cell-restricted intracellular antigen-related protein. J. Biol. Chem. 280, 1931–1943. [PubMed: 15536087]

Kedde M, van Kouwenhove M, Zwart W, Oude Vrielink JA, Elkon R, and Agami R (2010). A Pumilio-induced RNA structure switch in p27-3' UTR controls miR-221 and miR-222 accessibility. Nat. Cell Biol. 12, 1014–1020. [PubMed: 20818387]

Kiebler MA, and Bassell GJ (2006). Neuronal RNA granules: movers and makers. Neuron 51, 685–690. [PubMed: 16982415]

Kim YT, Hur EM, Snider WD, and Zhou FQ (2011). Role of GSK3 Signaling in Neuronal Morphogenesis. Front. Mol. Neurosci. 4, 48. [PubMed: 22131966]

Kislauskis EH, Zhu X, and Singer RH (1994). Sequences responsible for intracellular localization of beta-actin messenger RNA also affect cell phenotype. J. Cell Biol. 127, 441–451. [PubMed: 7929587]

Knott SRV, Maceli A, Erard N, Chang K, Marran K, Zhou X, Gordon A, Demerdash OE, Wagenblast E, Kim S, et al. (2014). A computational algorithm to predict shRNA potency. Mol. Cell 56, 796–807. [PubMed: 25435137]

Koshkin AA, Singh SK, Nielsen P, Rajwanshi VK, Kumar R, Meldgaard M, Olsen CE, and Wengel J (1998). LNA (Locked Nucleic Acids): Synthesis of the adenine, cytosine, guanine, 5-methylcytosine, thymine and uracil bicyclonucleoside monomers, oligomerisation, and unprecedented nucleic acid recognition. Tetrahedron 54, 3607–3630.

Leibovich L, Paz I, Yakhini Z, and Mandel-Gutfreund Y (2013). DRIMust: a web server for discovering rank imbalanced motifs using suffix trees. Nucleic Acids Res. 41, W174–179. [PubMed: 23685432]

Lois C, Hong EJ, Pease S, Brown EJ, and Baltimore D (2002). Germline transmission and tissue-specific expression of transgenes delivered by lentiviral vectors. Science 295, 868–872. [PubMed: 11786607]

Love MI, Huber W, and Anders S (2014). Moderated estimation of fold change and dispersion for RNA-seq data with DESeq2. Genome Biol. 15, 550. [PubMed: 25516281]

Marrero E, Rossi SG, Darr A, Tsoulfas P, and Rotundo RL (2011). Translational regulation of acetylcholinesterase by the RNA-binding protein Pumilio-2 at the neuromuscular synapse. J. Biol. Chem. 286, 36492–36499. [PubMed: 21865157]

Miao L, Yang L, Huang H, Liang F, Ling C, and Hu Y (2016). mTORC1 is necessary but mTORC2 and GSK3beta are inhibitory for AKT3-induced axon regeneration in the central nervous system. Elife 5, el4908.

Minis A, Dahary D, Manor O, Leshkowitz D, Pilpel Y, and Yaron A (2014). Subcellular transcriptomics-dissection of the mRNA composition in the axonal compartment of sensory neurons. Dev. Neurobiol. 74, 365–381. [PubMed: 24127433]

Morris AR, Mukherjee N, and Keene JD (2008). Ribonomic analysis of human Pum1 reveals cis-trans conservation across species despite evolution of diverse mRNA target sets. Mol. Cell. Biol. 28, 4093–4103. [PubMed: 18411299]

Park JW, Vahidi B, Taylor AM, Rhee SW, and Jeon NL (2006). Microfluidic culture platform for neuroscience research. Nat. Protoc. 1, 2128–2136. [PubMed: 17487204]

Pique M, Lopez JM, Foissac S, Guigo R, and Mendez R (2008). A combinatorial code for CPE-mediated translational control. Cell 132, 434–448. [PubMed: 18267074]

Quenault T, Lithgow T, and Traven A (2011). PUF proteins: repression, activation and mRNA localization. Trends Cell Biol. 21, 104–112. [PubMed: 21115348]

Schindelin J, Arganda-Carreras I, Frise E, Kaynig V, Longair M, Pietzsch T, Preibisch S, Rueden C, Saalfeld S, Schmid B, et al. (2012). Fiji: an open-source platform for biological-image analysis. Nat. Methods 9, 676–682. [PubMed: 22743772]

Shav-Tal Y, and Singer RH (2005). RNA localization. J. Cell Sci. 118, 4077–4081. [PubMed: 16155250]

Shigeoka T, Jung H, Jung J, Turner-Bridger B, Ohk J, Lin JQ, Amieux PS, and Holt CE (2016). Dynamic Axonal Translation in Developing and Mature Visual Circuits. Cell 166, 181–192. [PubMed: 27321671]

Siemen H, Colas D, Heller HC, Brustle O, and Pera RA (2011). Pumilio-2 function in the mouse nervous system. PLoS One 6, e25932. [PubMed: 22016787]

Soneson C, Love MI, and Robinson MD (2015). Differential analyses for RNA-seq: transcript-level estimates improve gene-level inferences. F1000Res 4, 1521. [PubMed: 26925227]

Spassov DS, and Jurecic R (2002). Cloning and comparative sequence analysis of PUM1 and PUM2 genes, human members of the Pumilio family of RNA-binding proteins. Gene 299, 195–204. [PubMed: 12459267]

Spillane M, Ketschek A, Merianda TT, Twiss JL, and Gallo G (2013). Mitochondria coordinate sites of axon branching through localized intra-axonal protein synthesis. Cell Rep. 5, 1564–1575. [PubMed: 24332852]

Taliaferro JM, Vidaki M, Oliveira R, Olson S, Zhan L, Saxena T, Wang ET, Graveley BR, Gertler FB, Swanson MS, et al. (2016). Distal Alternative Last Exons Localize mRNAs to Neural Projections. Mol. Cell 61, 821–833. [PubMed: 26907613]

Taylor AM, Blurton-Jones M, Rhee SW, Cribbs DH, Cotman CW, and Jeon NL (2005). A microfluidic culture platform for CNS axonal injury, regeneration and transport. Nat. Methods 2, 599–605. [PubMed: 16094385]

Terenzio M, Koley S, Samra N, Rishal I, Zhao Q, Sahoo PK, Urisman A, Marvaldi L, Oses-Prieto JA, Forester C, et al. (2018). Locally translated mTOR controls axonal local translation in nerve injury. Science 359, 1416–1421. [PubMed: 29567716]

tom Dieck S, Kochen L, Hanus C, Heumuller M, Bartnik I, Nassim-Assir B, Merk K, Mosler T, Garg S, Bunse S, et al. (2015). Direct visualization of newly synthesized target proteins in situ. Nat. Methods 12, 411–414. [PubMed: 25775042]

Van Etten J, Schagat TL, Hrit J, Weidmann CA, Brumbaugh J, Coon JJ, and Goldstrohm AC (2012). Human Pumilio proteins recruit multiple deadenylases to efficiently repress messenger RNAs. J. Biol. Chem. 287, 36370–36383. [PubMed: 22955276]

Vessey JP, Amadei G, Burns SE, Kiebler MA, Kaplan DR, and Miller FD (2012). An asymmetrically localized Staufen2-dependent RNA complex regulates maintenance of mammalian neural stem cells. Cell Stem Cell 11, 517–528. [PubMed: 22902294]

Vessey JP, Schoderboeck L, Gingl E, Luzi E, Riefler J, Di Leva F, Karra D, Thomas S, Kiebler MA, and Macchi P (2010). Mammalian Pumilio 2 regulates dendrite morphogenesis and synaptic function. Proc. Natl. Acad. Sci. U. S. A. 107, 3222–3227. [PubMed: 20133610]

Vessey JP, Vaccani A, Xie Y, Dahm R, Karra D, Kiebler MA, and Macchi P (2006). Dendritic localization of the translational repressor Pumilio 2 and its contribution to dendritic stress granules. J. Neurosci. 26, 6496–6508. [PubMed: 16775137]

Villarin JM, McCurdy EP, Martinez JC, and Hengst U (2016). Local synthesis of dynein cofactors matches retrograde transport to acutely changing demands. Nat. Commun. 7, 13865. [PubMed: 28000671]

Wang X, McLachlan J, Zamore PD, and Hall TM (2002). Modular recognition of RNA by a human pumilio-homology domain. Cell 110, 501–512. [PubMed: 12202039]

Weidmann CA, Raynard NA, Blewett NH, Van Etten J, and Goldstrohm AC (2014). The RNA binding domain of Pumilio antagonizes poly-adenosine binding protein and accelerates deadenylation. RNA 20, 1298–1319. [PubMed: 24942623]

White EK, Moore-Jarrett T, and Ruley HE (2001). PUM2, a novel murine puf protein, and its consensus RNA-binding site. RNA 7, 1855–1866. [PubMed: 11780640]

Xing L, and Bassell GJ (2013). mRNA localization: an orchestration of assembly, traffic and synthesis. Traffic 14, 2–14. [PubMed: 22913533]

Xu EY, Chang R, Salmon NA, and Reijo Pera RA (2007). A gene trap mutation of a murine homolog of the Drosophila stem cell factor Pumilio results in smaller testes but does not affect litter size or fertility. Mol. Reprod. Dev. 74, 912–921. [PubMed: 17219433]

Zappulo A, van den Bruck D, Ciolli Mattioli C, Franke V, Imami K, McShane E, Moreno-Estelles M, Calviello L, Filipchyk A, Peguero-Sanchez E, et al. (2017). RNA localization is a key determinant of neurite-enriched proteome. Nat. Commun. 8, 583. [PubMed: 28928394]

Zhang M, Chen D, Xia J, Han W, Cui X, Neuenkirchen N, Hermes G, Sestan N, and Lin H (2017). Post-transcriptional regulation of mouse neurogenesis by Pumilio proteins. Genes Dev. 31, 1354–1369. [PubMed: 28794184]

Zheng JQ, Kelly TK, Chang B, Ryazantsev S, Rajasekaran AK, Martin KC, and Twiss JL (2001). A functional role for intra-axonal protein synthesis during axonal regeneration from adult sensory neurons. J. Neurosci. 21, 9291–9303. [PubMed: 11717363]

Highlights

- Presence of a PBE negatively regulates mRNA localization/translation
- Pum2 retains PBE-containing mRNAs in the soma
- Developmental regulation of Pum2 controls axonal transcriptome composition
- Pum2 function is required for proper axon branching/outgrowth in vivo

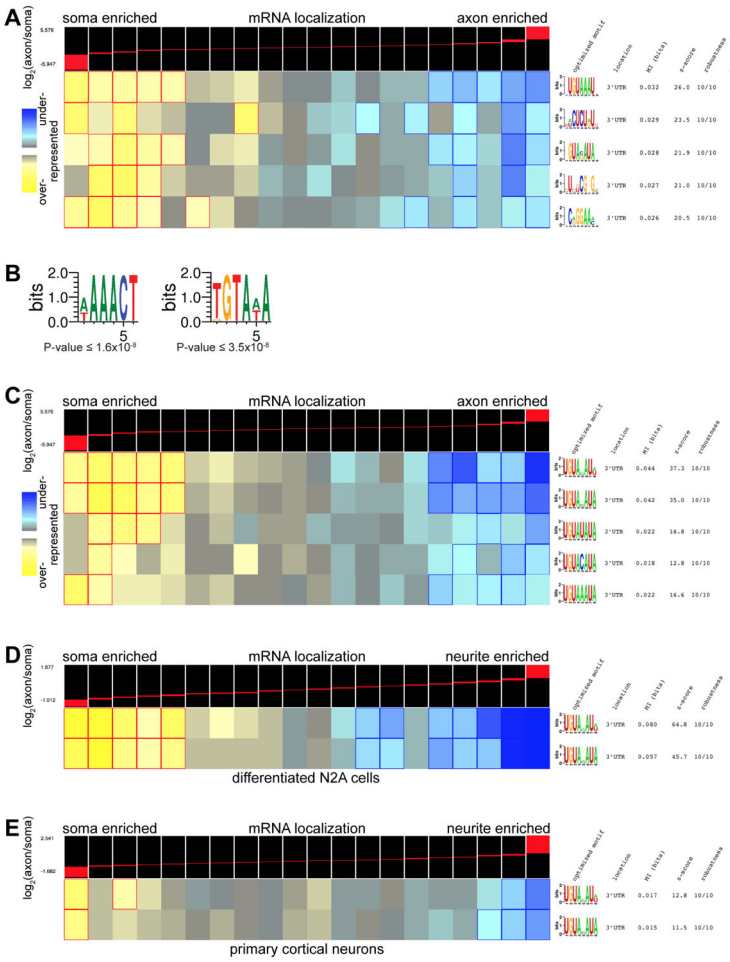

Figure 1. Presence of a PBE is predictive for soma versus axon localization of mRNAs

(A) FIRE motif discovery was run in 'discovery mode' on a transcriptome set from mouse embryonic DRG neurons to identify soma or axon enriched sequence elements. The top five identified motifs are shown. Bins to the left contain mRNAs that are enriched in cell bodies, while the bins on the right contain mRNAs enriched in axons. Each bin contains about 200 mRNAs. Yellow to blue color scale signifies the degree of enrichment or depletion, respectively, of a motif in a category/bin where significant events ($p<0.05$) are marked by red or blue frames.

(B) 3'UTR sequences of the top 100 somatically and axonally enriched mRNAs were used in DRIMust motif discovery. The algorithm was run in the default mode allowing for motifs to be from 5 to 10 nucleotides in size and the minimum statistical threshold was set at 10^{-6}.

(C) FIRE was run in 'non-discovery mode' to test the two variants of the PBE motifs: UGUA[ACU]AU[AU] (Pum2 preferred; top row) and UGUA[ACU]AUA (Pum1 and Pum2; second row). Additionally, PBEs with variations in their 5th position were tested: UGUA[ACU]AUA, UGUAAAUA, UGUAUAUA, UGUACAUA, UGUAGAUA. Only motifs found to be significant are shown.

(D) FIRE was run in 'non-discovery mode' on a genome-wide subcellular localization dataset from N2A neuroblastoma cells. The two variants of the PBE were tested,

UGUA[ACU]AU[AU] (Pum2 preferred; top row) and UGUA[ACU]AUA (Pum1 and Pum2; second row).

(E) FIRE was run in ‘non-discovery mode’ on primary cortical neuron genome-wide subcellular localization measurement dataset. The two variants of the PBE were tested, UGUA[ACU]AU[AU] (Pum2 preferred; top row) and UGUA[ACU]AUA (Pum1 and Pum2; second row).

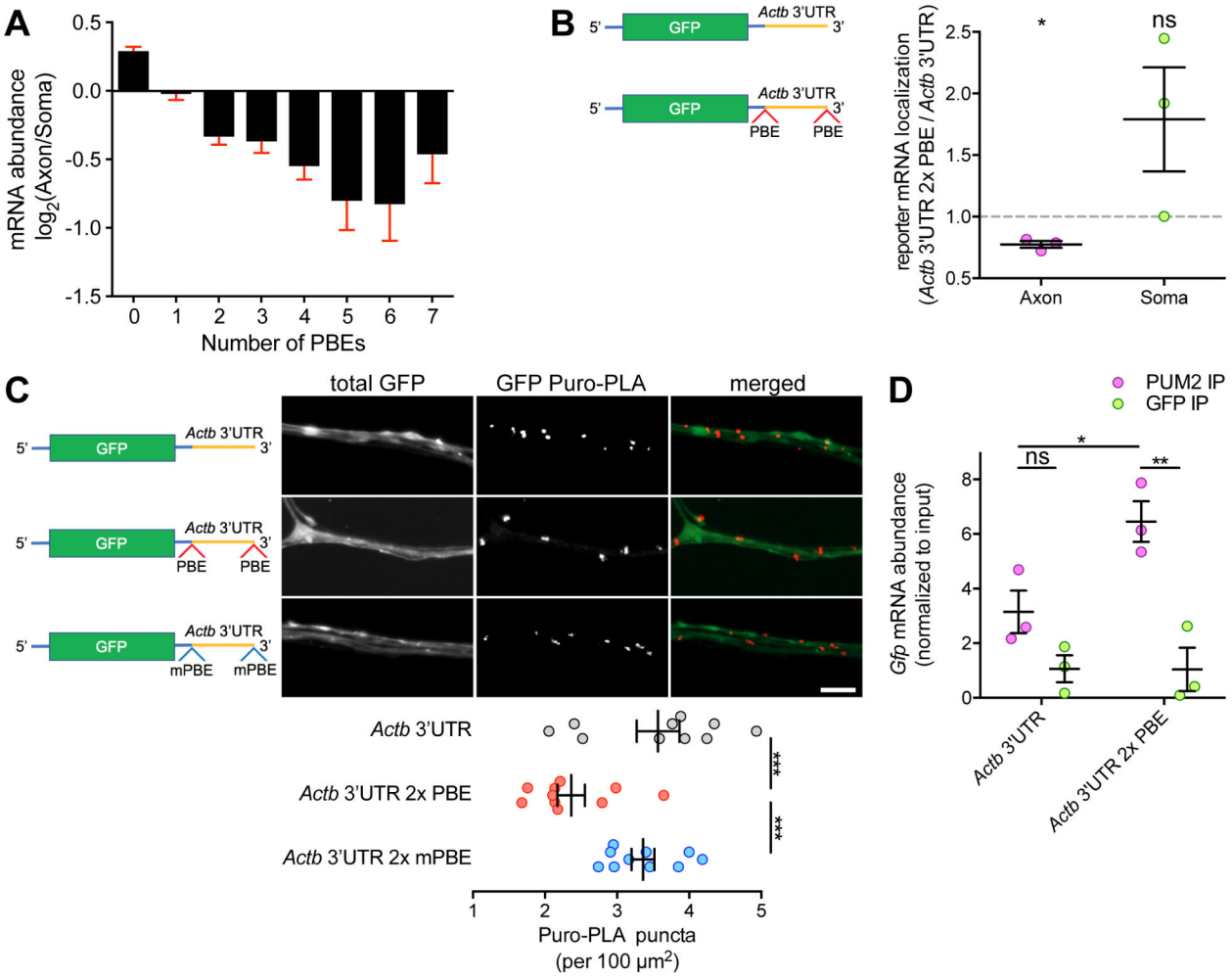

Figure 2. PBEs are sufficient to restrict axonal mRNA localization and translation

(A) Distribution plot of top 50th percentile of mRNAs analyzed with DESeq2 from embryonic mouse DRG neuronal transcriptome by number of PBE elements in the 3'UTRs.

(B) Rat embryonic neurons grown in microfluidic devices were infected with lentiviruses driving the expression a GFP reporter mRNA containing the *Actb* 3'UTR with or without two flanking PBEs. Reporter mRNA expression levels were measured in axons by qRT-PCR and normalized to the condition without the PBE. Means ± SEM; n = 3 independent experiments. One sample t-test for difference to theoretical mean of 1.0. *p<0.05; ns, not significant.

(C) Rat embryonic rat neurons grown in microfluidic devices were infected with lentiviruses driving the expression a GFP reporter mRNA containing the *Actb* 3'UTR with or without two flanking PBEs or mutated PBEs. Axonal GFP synthesis was measured over 10 minutes using a Puro-PLA. Means ± SEM of 10 optical fields; n = 3 independent experiments. One-way ANOVA with Dunnett's multiple comparisons test. ***p<0.001. Scale bar, 10 µm.

(D) HEK293T cells were co-transfected with Pum2 and reporter mRNA with or without the PBE. Pum2 or GFP were immunoprecipitated and pulled-down reporter mRNA was

measured using qRT-PCR. Means ± SEM; n = 3 biological replicates. Two-way ANOVA with Sidak's multiple comparisons test. *p<0.05; **p<0.01; ns, not significant.

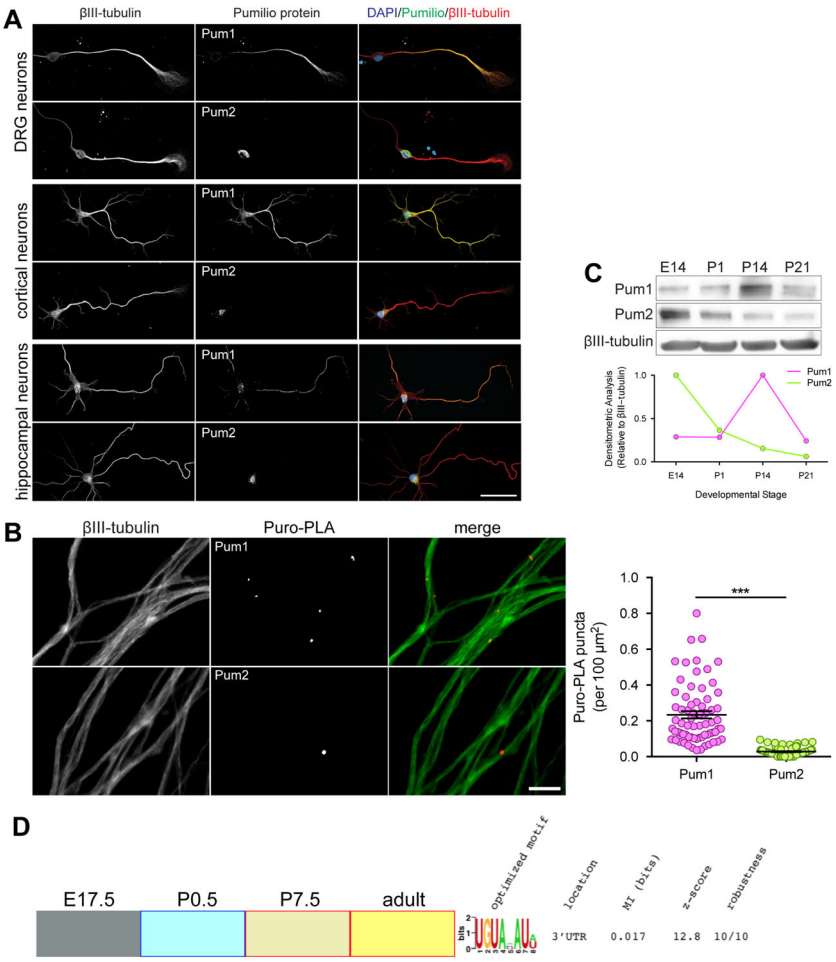

Figure 3. Pum1 and Pum2 are differentially expressed

(A) Rat embryonic DRG, cortical, and hippocampal neurons were immunostained with antibodies directed against Pum1 or Pum2 and βIII-tubulin. Scale bar, 25 μm.

(B) Puro-PLA for Pum1 and Pum2 was performed on rat embryonic DRG neurons and quantified in axons. Means ± SEM of 70-80 optical fields; n = 3 biological replicates. Unpaired t-test. ***p<0.001. Scale bar, 10 μm.

(C) Mouse brain cortical lysates from different developmental stages were immunoblotted for Pum1 and Pum2. Pumilio levels were quantified and normalized to βIII-tubulin.

(D) FIRE was run on 'non-discovery mode' with UGUA[ACU]AU[AU], the Pum2 preferred motif, as the test motif on a dataset of groups of mRNAs translated in mouse axons at different developmental stages.

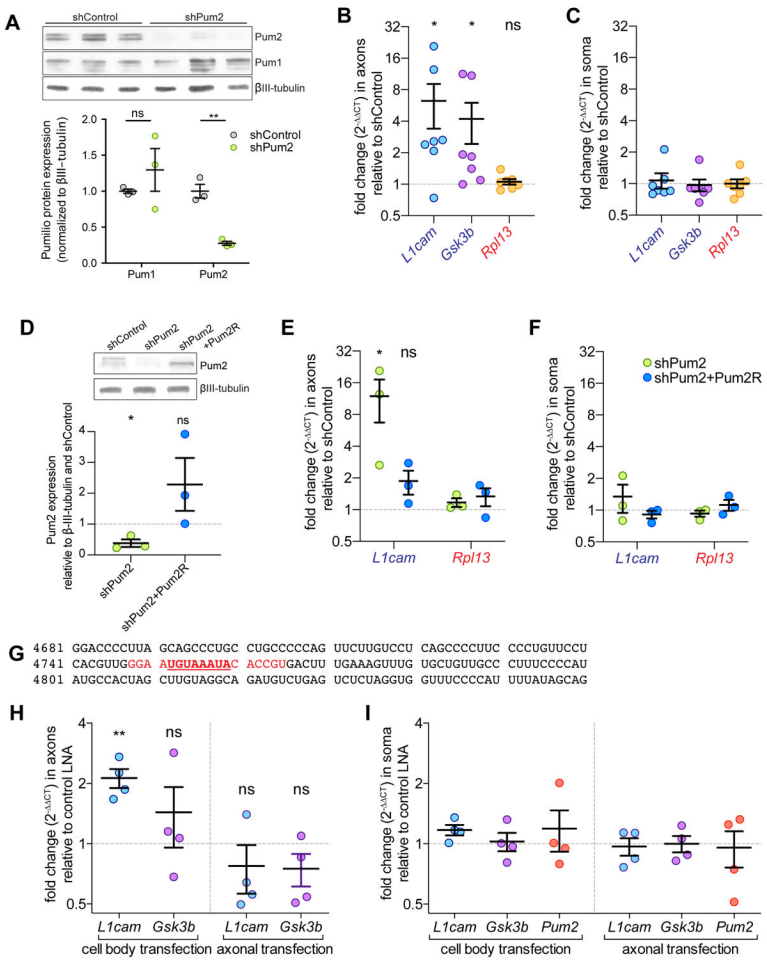

Figure 4. Pum2 knockdown causes increased axonal localization of L1cam transcripts

(A) Rat embryonic DRG neurons were transduced with shControl or shPum2, and the levels of Pumilio proteins were determined by immunoblotting seven days later. Means ± SEM; n = 3 biological replicates. Unpaired t-tests. **p<0.01; ns, not significant.

(B) Rat embryonic DRG neurons grown in microfluidic chambers were transduced with shControl or shPum2 on DIV0. Seven days later, the axonal and somatic material was harvested separately. qRT-PCR with preamplification was used to measure the relative levels of *L1cam, Gsk3b* (Pum2 targets), and *Rpl13* (non-target) mRNA in axons. mRNA levels are shown as fold change ($2^{\Delta\Delta CT}$) compared to shControl, indicated with a dotted line at 1. Values are displayed on a log2 scale. Blue font = Pum2 target, red font = non-target. Means ± SEM; n = 7 independent experiments. Paired t-tests comparing ΔCT of shControl and shPum2 conditions for each qPCR target normalized to the housekeeping gene *Rps19*. *p<0.05; ns, not significant.

(C) Somatic qRT-PCR for the same experiment shown in (B).

(D) Rat embryonic DRG neurons were grown in microfluidic chambers and transduced with shControl or shPum2 on DIV0, followed by Pum2R transduction on DIV3. Somatic material was collected on DIV7. The levels of Pum2 were determined by immunoblotting and normalized to levels of βIII-tubulin and the respective shControl sample. Means ± SEM; n =

3 biological replicates. One-sample t-test for difference to theoretical mean of 1.0. *p<0.05; ns, not significant.

(E) Using the experimental strategy described in (D), axonal and somatic RNA was harvested separately on DIV7. qRT-PCR with preamplification was used to measure the relative levels of *L1cam* and *Rpl13* mRNA in axons. mRNA levels are shown as fold change ($2^{-\Delta\Delta CT}$) compared to shControl, indicated with a dotted line at 1. Values are displayed on a log2 scale. Blue font = Pum2 target, red font = non-target. Means ± SEM; n = 3 independent experiments. Paired t-tests comparing ΔCT of shControl and shPum2 conditions for each qPCR target normalized to the housekeeping gene *Rps19*. *p<0.05; ns, not significant.

(F) Somatic qRT-PCR for the same experiment shown in (E).

(G) Partial 3'UTR of rat *L1cam*. The binding region of the targeting LNA is indicated in red, and the PBE (UGUAAAUA) is in bold and underlined.

(H) Rat embryonic DRG neurons were grown in microfluidic chambers and either the cell body or the axonal compartments were transfected with non-targeting control or *L1cam* PBE-targeting LNAs on DIV5. After 48 hours, somatic and axonal RNA was collected separately. qRT-PCR with preamplification was used to measure the relative levels of *L1cam* and *Gsk3b* mRNA in axons. mRNA levels are shown as fold change ($2^{-\Delta\Delta CT}$) compared to non-targeting LNAs, indicated with a dotted line at 1. Values are displayed on a log2 scale. Means ± SEM, n= 4 independent experiments. Paired t-tests comparing ΔCT of control and targeting LNA conditions for each qPCR target normalized to the housekeeping gene *Rps19* **p<0.01; ns, not significant.

(I) Somatic qRT-PCR from the same experiments shown in (H).

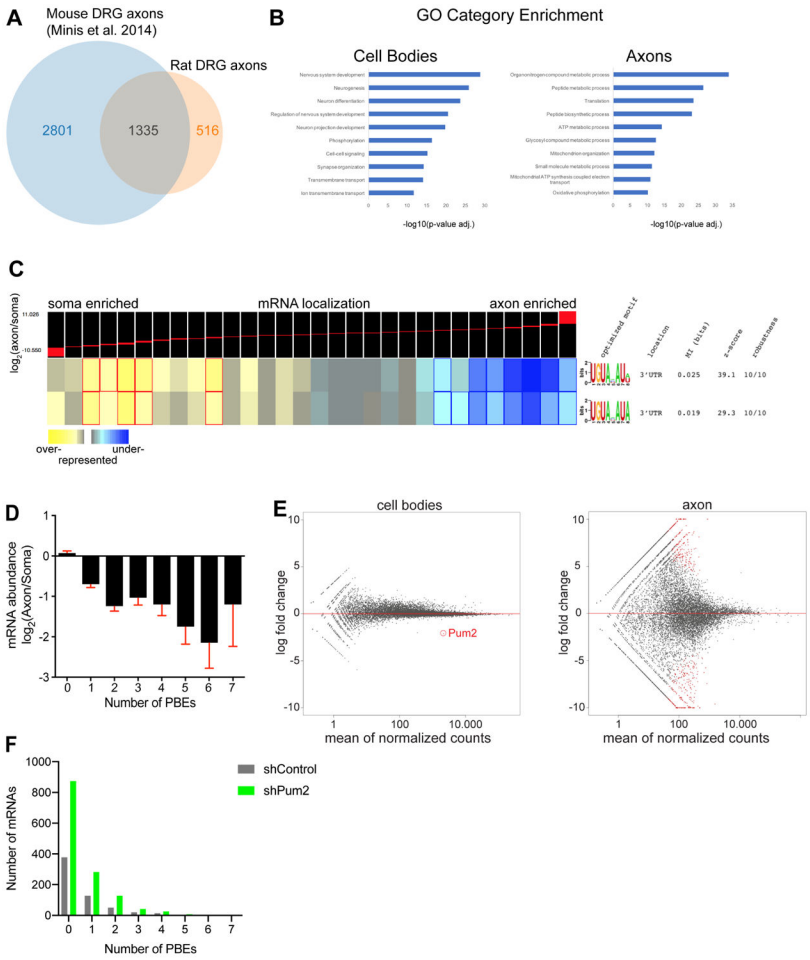

Figure 5. Pum2 knockdown changes axonal but not somatic transcriptome

(A) Rat embryonic DRG neurons were grown in microfluidic chambers and the axonal and cell body transcriptomes were determined by RNAseq. Venn diagram depicting the overlap between the third quartile of mRNAs detected by RNAseq in axons from rat sensory neurons (this work) and a previously published transcriptome of mouse sensory neuron axons.

(B) Gene ontology enrichment analysis of mRNAs enriched in either cell bodies or axons.

(C) FIRE was run in 'non-discovery mode' to test the two variants of the PBE motifs: UGUA[ACU]AU[AU] (Pum2 preferred; top row) and UGUA[ACU]AUA (Pum1 and Pum2; second row) on the transcriptome sets from rat sensory neurons grown in microfluidic devices.

(D) Distribution plot of top 50th percentile of mRNAs (6,000) analyzed with DESeq2 from embryonic rat DRG neuronal transcriptome by number of PBE elements in the 3'UTRs.

(E) DIV7 sensory rat neurons grown in microfluidic chambers and transduced with either shControl or shPum2 were subjected to RNA-Seq. MA Plot reveals differential expression of mRNAs in neuronal cell bodies (left) and axons (right) between the two conditions.

(F) Distribution of significantly changed axonal mRNAs (p-value < 0.05) from DESeq2 analysis of shControl vs shPum2 by the number of PBEs in the 3'UTRs.

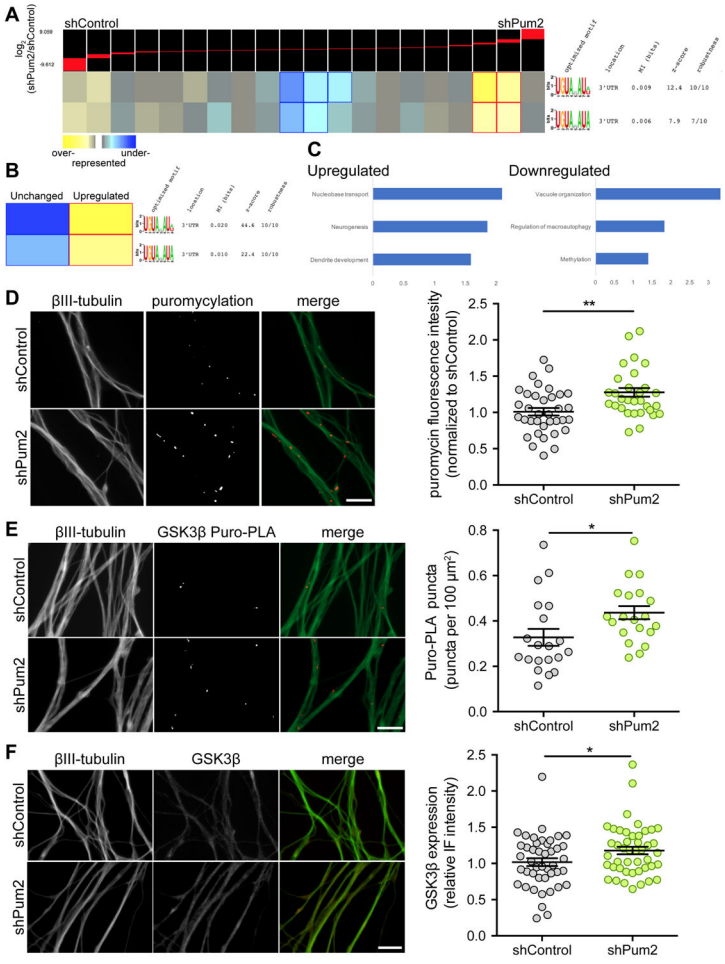

Figure 6. Pum2 knockdown increases axonal localization of mRNAs containing PBEs

(A) FIRE was run in 'non-discovery mode' to test the two variants of the PBE motifs: UGUA[ACU]AU[AU] (Pum2 preferred; top row) and UGUA[ACU]AUA (Pum1 and Pum2; second row) on the dataset of axonal transcriptome changes in response to shPum2 versus shControl expression.

(B) FIRE was run in 'non-discovery mode' to test the two variants of the PBE motifs: UGUA[ACU]AU[AU] (Pum2 preferred; top row) and UGUA[ACU]AUA (Pum1 and Pum2; second row) on two sets of mRNAs, one representing mRNAs whose expression did not change in axons upon Pum2 knockdown, while the other is the set of mRNAs that were increased.

(C) GO term analysis of the mRNAs up- or downregulated in axons upon Pum2 knockdown.

(D) Axons of DIV7 rat sensory neurons treated with shControl or shPum2 were labeled with puromycin for 10 mins to detect newly synthesized proteins and immunostained with α-Puromycin (red) and α-βIII Tubulin (green) (n=3 biological replicates). Unpaired t-test. ** $p < 0.01$. Scale bar, 10 μm.

(E) Puro-PLA against GSK3β in axons of rat embryonic DRG neurons expressing either shControl or shPum2. Means ± SEM of 20 optical fields; n = 3 biological replicates. Unpaired t-test. *$p<0.05$.

(F) Immunostaining against GSK3β in axons of rat embryonic DGR neurons expressing either shControl or shPum2. Means ± SEM of 44-45 optical fields; n = 3 biological replicates. Unpaired t-test. *p<0.05.

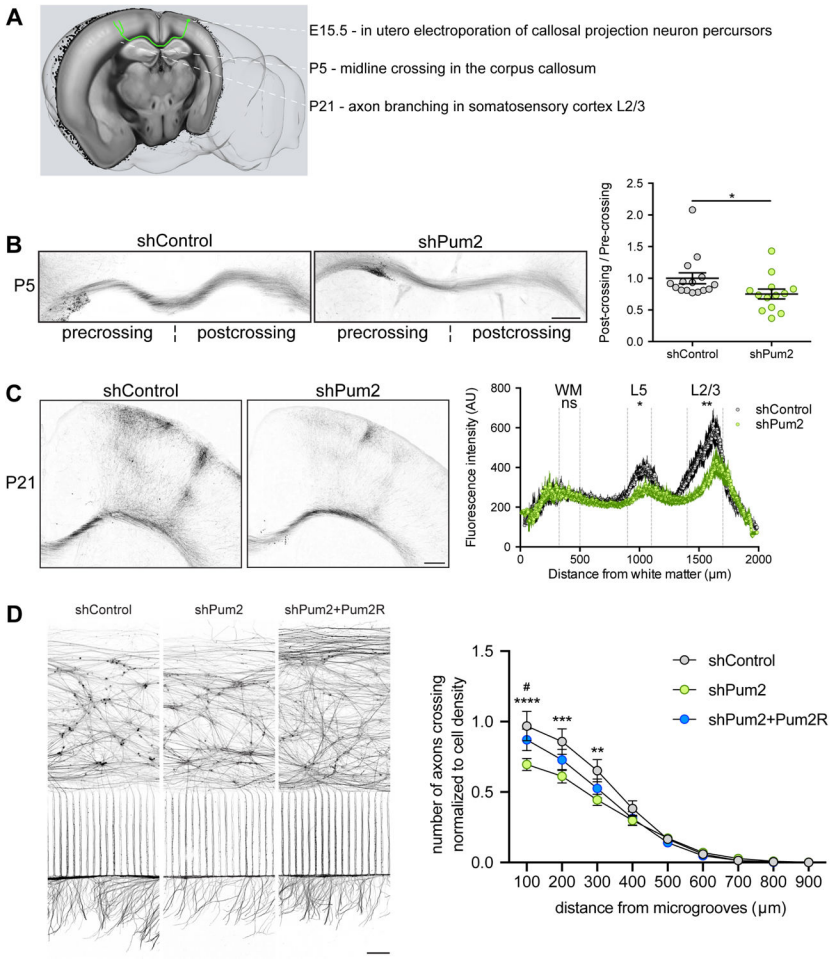

Figure 7. Pum2 knockdown interferes with axon growth and branching

(A) Experimental scheme: shControl and shPum2 expression plasmids were delivered to E15.5 mouse embryos cortices by in utero electroporation. The mice were sacrificed 5 days (P5) or 3 weeks (P21) after birth, their brains vibratome sectioned and axons visualized via expression of ZsGreen (contained in shRNA constructs).

(B) Visualization and quantification of GFP fluorescence intensity (optical density related to axon density) at the corpus callosum at P5. Means ± SEM of 13-15 sections; n = 2 independent in utero electroporations. Unpaired t-test. *p<0.05. Scale bar, 500 μm.

(C) Visualization and quantification of GFP fluorescence intensity (i.e. axon density) in cortical layers of the contralateral hemisphere. GFP fluorescence intensities are normalized to the white matter, to account for different labeling efficiencies. Means ± SEM of 5-7 brains; n = 3 independent in utero electroporations. Average intensities in WM, L5, and L2/3 were compared by unpaired t-tests. **p<0.01; *p<0.05. Scale bar, 500 μm.

(D) Rat embryonic DRG neurons were cultured in microfluidic chambers and transduced with shControl or shPum2 constructs (DIV0) and Pum2R construct (DIV2). The axons were severed by aspiration on DIV5 and allowed to regrow for 24 hours. Cells were immunostained for β-III-tubulin and the number of axons crossing lines at various distances from the microgrooves was quantified and normalized to the average cell density in each chamber. Means ± SEM of 23-24 optical fields from 7-8 microfluidic chambers per

condition; n = 3 biological replicates. Two-way ANOVA with Bonferroni's multiple comparisons tests. Asterisks (*) indicate shControl vs. shPum2; pound symbol (#) indicates shPum2 vs. shPum2+Pum2R.****p<0.0001; ***p<0.001; **p<0.01; #p<0.05. Scale bar, 200 μm.

Table 1.

List of mRNAs most strongly regulated in axons upon *Pum2* knockdown

10 most upregulated mRNAs in axons upon Pum2 knockdown						
mRNA	**base mean**	**log_2-fold change**	**log_2-fold change standard error**	**p value**	**adjusted p value**	**PBE in 3'UTR**
Mmpl0	869.6610	9.0595	1.7752	3.33E-07	0.000341	no
Rhov	138.2151	8.4680	1.8331	3.85E-06	0.001317	no
Naa40	142.4338	8.3556	1.8764	8.47E-06	0.001924	no
Cds1	151.4677	7.9927	1.9475	4.06E-05	0.005286	yes
Slc35d2	90.18398	7.7969	1.8990	4.03E-05	0.005286	no
Myot	87.81515	7.7441	1.9065	4.86E-05	0.005650	no
Arhgap24	119.566	7.5830	1.9854	0.000134	0.010305	yes
Sprr1a	166.4196	7.5784	2.0128	0.000166	0.011608	yes
Msr1	113.3206	7.5124	1.9907	0.000161	0.011581	yes
Atp6v0d2	297.5639	7.4906	1.4699	3.47E-07	0.000341	yes
10 most downregulated mRNAs in axons upon Pum2 knockdown						
mRNA	**base mean**	**log_2-fold change**	**log_2-fold change standard error**	**p value**	**adjusted p value**	**PBE in 3'UTR**
Tec	295.5738	−9.6122	1.7830	7.01E-08	0.000191	yes
Gtf2b	305.523	−9.5826	1.7960	9.53E-08	0.000191	yes
Sh2b2	217.3802	−9.1542	1.8189	4.83E-07	0.000389	no
Il2rg	478.2237	−9.1446	1.5793	7.03E-09	6.23E-05	no
Cox11	203.5260	−9.05375	1.8273	7.25E-07	0.000535	no
Ccl22	315.5188	−8.98647	1.8951	2.12E-06	0.000893	no
Trmu	242.2106	−8.61794	1.9213	7.28E-06	0.001842	no
Tcp11l2	479.9264	−8.48569	1.7760	1.77E-06	0.000861	no
Rab20	418.1634	−8.39550	1.5581	7.12E-08	0.000191	no
Alg12	154.6612	−8.27186	1.9268	1.76E-05	0.003200	no

The ten most up- or downregulated mRNAs in axons of DRGs neurons upon Pum2 knockdown are listed with the DESeq2 output. Presence or absence of at least one PBE in their 3'UTRs is indicated.